A collaborative study on temperature diurnal tide in the midlatitude mesopause region (41°N, 105°W) with Na lidar and TIMED/SABER observations

Tao Yuan [a,*], Chiao-Yao She [a], David Krueger [a], Steven C. Reising [a], Xiaoli Zhang [b], Jeffrey M. Forbes [b]

[a] Utah State University, Logan, UT 84322-4415, USA
[b] University of Colorado, Boulder, CO 80309-0429, USA

ARTICLE INFO

ABSTRACT

The na lidar-observed temperature diurnal tidal perturbations, based on full-diurnal-cycle observations from 2002 to 2008, are compared with tidal wave measurements by the TIMED/SABER instrument to elucidate the nature of diurnal tidal-period perturbations observed locally. The diurnal amplitude and phase profiles deduced by the two instruments are in very good agreement most of the year. However, the lidar-observed diurnal amplitudes during winter months and early spring are considerably larger than SABER observations, leading to the existence of a significant amplitude maximum of 12 K near 90 km in February and a different seasonal structure of temperature diurnal amplitude from the two instruments. The lidar-observed diurnal phase shows propagating wave characteristics during equinoctial months, but exhibit "evanescent wave" behavior in winter months, whereas SABER diurnal tidal phase exhibits propagating diurnal tidal character all year long with small seasonal variation. This anomalous tidal characteristic from the lidar observations repeats almost every winter. The exact mechanism behind this tidal feature is not fully understood, therefore further investigation and more experimental observations are necessary.

1. Introduction

Solar thermal tidal waves are global scale waves that are harmonics of a solar day, consistently modulating the MLT (Mesosphere and Lower Thermosphere) region of the atmosphere with considerable amplitudes, and are one of the most important dynamic effects within the middle and upper atmosphere. Among them, the migrating tides, which are mostly generated due to solar energy absorption by water vapor in the troposphere and ozone in the stratosphere and, therefore, synchronized with the relative motion of sun, have been known as the dominant tidal component within most parts of the MLT region (Chapman and Lindzen, 1970, Forbes and Garrett, 1978). Its seasonal variations within this region are largely controlled by the combination of the variation in solar heating and zonal mean winds (McLandress, 2002). Hagan (1996) pointed out that the seasonal variations of the phase difference between IR (infrared by water vapor within troposphere) and UV (ultraviolet by ozone within stratosphere) forcing could also impact the seasonal change of tidal wave amplitudes. The nonmigrating (not sun synchronous) tides were

also thought to be an important contributor to tidal variability in the MLT region (Forbes and Garrett, 1979; Kato, 1980; Forbes, 1984, 1995; Volland, 1988; Hagan, 2000). The invaluable satellite observations during the past decade (Talaat and Lieberman, 1999; Oberheide et al., 2006; Wu et al., 2008; Forbes and Wu, 2006; Forbes et al., 2008), provide signatures of nonmigrating tides, resulting in their intensive investigation giving insight to tidal wave modulations of the mean atmosphere. However, the tidal forcing for nonmigrating tides is complex. The latent heat released due to rain drop formation in the troposphere is long-known to be one major nonmigrating tidal source (Lindzen, 1978; Hong and Wang, 1980; Forbes et al., 1997; Hagan et al., 1997; Hagan and Forbes, 2002). In addition, nonlinear interactions of migrating tidal waves with global scale planetary waves (Miyahara and Miyoshi, 1997; Hagan and Roble, 2001; Mclandress, 2001; Mayr et al., 2003; Lieberman et al., 2004) and with gravity waves (Mclandress and Ward, 1994; Walterscheid, 1981; Mayr et al., 2001) can also excite significant nonmigrating tidal components.

From a single ground-based station (Tsuda et al., 1988; Vincent et al., 1989; Manson et al., 1989; Avery et al., 1989; Franke and Thorsen, 1993), one may easily observe local oscillations of atmospheric variables at sub-harmonics of the diurnal frequency but is unable to identify whether these oscillations are global

* Corresponding author. Tel.: +1 970 491 5646.
E-mail address: titus@lamar.colostate.edu (T. Yuan).

(migrating or nonmigrating) wave modulations, local oscillations, or superposition of the two. The characteristics of solar tidal waves may be deduced either from full-diurnal-cycle observations near the same latitude but at multiple longitudes, or from the combination of satellite observations, providing partial local-time global coverage, and ground-based full-diurnal-cycle observations at a fixed location. However, these joint observations are rare, especially for temperature diurnal tidal wave studies due to the shortage of the full diurnal cycle temperature observations from ground-based stations. Colorado State University (CSU) Na lidar accomplished the full-diurnal-cycle observations of temperature, zonal and meridional winds within the mesopause region in May 2002. Since then, the system has accumulated close to 5000 h of data by 2008, part of which are used to deduce monthly climatologies of the mean temperature, zonal and meridional wind (Yuan et al., 2008a) and semidiurnal period tidal perturbations (Yuan et al., 2008b) of the three atmospheric parameters. Considerable data are necessary to extract major diurnal tidal modulations and to average out the transient variability due to interactions with gravity waves and due to modulation in mean-state by planetary waves (Liu et al., 2007). The Sounding of the Atmosphere using Broadband Emission Radiometry (SABER) instrument onboard the Thermosphere–Ionosphere–Mesosphere Energetic and Dynamics (TIMED) satellite has been able to sample atmospheric neutral temperature from 20–120 km above the surface on a global scale and, thus, provides a global view of temperature tidal wave structures (Zhang et al., 2006). In this paper, the monthly temperature diurnal tidal period perturbations measured by CSU Na lidar will be compared to the temperature diurnal tide deduced from TIMED/SABER measurements during almost the similar period, marking the first such comprehensive comparison between the tidal temperature wave observations from ground-based and satellite observations.

2. Data analysis

2.1. Colorado State University Na lidar

The technique for using CSU Na lidar data set to extract temperature tidal period perturbations is in a previous paper (She et al., 2002). The climatology of nocturnal temperature measurements by lidar was compared with TIMED/SABER observations (Xu et al., 2006), showing good agreement between the temperature measurements by the two instruments. Since May 2002, the CSU lidar has been upgraded, and is now capable of simultaneous temperature, zonal and meridional winds measurements over a full diurnal cycle (She et al., 2003). Full-diurnal cycle

lidar data distributions from 2002 to 2008 are listed in Table 1. Harmonic analysis is applied at each altitude of the hourly mean temperature profiles built from the data sets with continuous observations of 24 h or longer. In such analysis, the least-squares fitting method is done on such continuous hourly data to deduce the amplitude and phase of the monthly mean diurnal, semidiurnal, terdiurnal and quarterdiurnal tidal components simultaneously. For multi-year analysis, lidar observations within the same month of different years are binned according to the UT time sequence of respective years. Then harmonic analysis is performed to deduce the mean fields and tidal components. By doing so, short term variability is minimized and only consistent tidal signatures are retrieved.

2.2. TIMED/SABER

The TIMED satellite was launched on December 7th, 2001 and the SABER instrument began its observations in January 2002, just before the CSU Na lidar started its full diurnal cycle observations. SABER measures CO_2 infrared limb radiance from approximately 20 km to 120 km altitude and the kinetic temperature profiles are retrieved over these heights using a full non-LTE inversion (Mertens et al., 2001, 2004). The retrieval errors, in addition to those associated with instrumental noise, are estimated by Remsberg et al. (2008) and GarcíaComas et al. (2008). The method for extracting tidal waves from SABER temperature observations has been described in detail in a recent paper (Forbes et al., 2008). The uncertainty of the SABER tidal amplitudes varies from 0.6–0.9 K at 76 km to 2–3 K near 116 km. The SABER temperature measurements (version 1.07) between March 2002 and December 2007 are employed for the present study. However, due to the sampling rate of the TIMED satellite and the dual-node sampling of the SABER instrument, full 24 h coverage for each day is obtained from averaging over a 60 day window centered about that day with a horizontal interval of 24° in longitude, 5° in latitude. SABER tides with the vertical interval of 2 km, therefore, represent 60-day running means that are vector averaged into monthly mean composites for tidal analysis, which includes 13 diurnal-period global components with zonal wavenumbers from −6 to 6. The negative wavenumbers are for eastward propagating waves.

3. Temperature diurnal tidal seasonal variations by lidar and TIMED/SABER

3.1. SABER reconstructed diurnal tidal comparisons with lidar

To compare the satellite and ground-based tidal observations, we reconstruct the total diurnal tidal wave modulations as the superposition of the SABER migrating (DW1) plus nonmigrating tides of wavenumbers from −6 to +6 evaluated near the lidar site at 40° N, 255°E. Because of the 60-day running means, these should provide the representative tidal wave characteristics over the ground based station without the day-to-day tidal variability.

Fig. 1 shows comparisons between the amplitude profiles of temperature diurnal tidal period perturbation observed by CSU Na lidar (asterisks) and the reconstructed temperature diurnal tidal amplitude (solid line) at 40°N, 255°E deduced from SABER. Also, the migrating component of temperature diurnal tide (DW1–dash line) is plotted, and we will discuss its contributions to total diurnal tide in the next section. From the comparisons between the lidar diurnal tidal period perturbations and the reconstructed total diurnal tide of SABER, the most salient feature of seasonal variations is the much larger amplitude observed by lidar from

Table 1
Number of hours of continuous observations for each month by CSU Na lidar from 2002 to 2008 with observation time longer than full diurnal cycle.

	2002	2003	2004	2005	2006	2007	2008	Total
January	N/A	60	N/A	117	53	103	32	365
February	N/A	40	73	N/A	134	41	28	316
March	N/A	117	96	N/A	N/A	N/A	N/A	213
April	N/A	83	95	N/A	N/A	65	54	297
May	108	39	72	96	N/A	N/A	N/A	315
June	56	147	36	73	N/A	N/A	N/A	312
July	85	68	60	187	49	N/A	34	483
August	83	92	100	N/A	36	32	56	399
September	70	241	83	144	78	103	N/A	719
October	73	95	57	92	97	113	83	610
November	88	107	70	N/A	77	N/A	61	403
December	70	128	76	N/A	132	N/A	N/A	406

Fig. 1. Temperature diurnal amplitude profiles from 80 to 105 km for each month of the year: TIMED/SABER reconstructed diurnal tide (solid line), TIMED/SABER migrating diurnal tide (dash line) and CSU Na lidar diurnal period perturbations (asterisks).

November to March within significant part of the mesopause region. The lidar diurnal tidal measurements show a dramatic maximum near 90 km in February with the peak amplitude over 12 K. This maximum, along with the 10 K peak value near 94 km altitude in March, forms a remarkable temperature diurnal amplitude peak. It is worth mentioning here that the lidar observed zonal wind diurnal tidal amplitude (not the topic of this paper) has quite similar seasonal variation with its significant maximum in February. Diurnal amplitudes within the mesopause region during summer months are small from the measurements of both instruments, with the minimum amplitude below 2 K near 85 km. SABER observations indicate a similar magnitude of tidal amplitude in winter solstice condition to that in the summer with the amplitude value of 2–3 K for most part of the region. Near equinoctial months (March and September), SABER diurnal amplitudes are around 6–7 K. This, along with the two minimum at solstice, gives rise to tidal seasonal variations that are in general agreement with earlier tidal model studies (Forbes, 1982a; Hagan et al., 1999). The lidar observations, as discussed above, show considerably larger winter diurnal amplitudes than in the summer months. In fact, the lidar observations show that the amplitude of temperature diurnal tidal perturbation, which stays near or above 6 K during the winter months, is about twice that of the amplitudes during summer months (less than 3 K). Therefore, winter solstice minimum of diurnal tidal amplitude as

predicted by classical theory and seen in the SABER data is not obvious in the lidar observations. This makes the annual variation dominant in lidar observed diurnal amplitude seasonal variation as opposed to a dominant semiannual variation observed in SABER and predicted by classical theory. The larger tidal amplitudes observed by CSU Na lidar (from January to March and October to December) could be because of an overestimation of the climatological mean due to inadequate sampling by the lidar or because of some local tidal-period oscillations that are captured by the lidar but missed by SABER due to its sampling scheme.

The associated monthly diurnal tidal phases are shown in Fig. 2. From lidar results (asterisks), one can easily see the seasonal variation of the temperature diurnal phase (vertical wavelength). The vertical wavelength is over 100 km in January and then drops to near 30 km around spring equinox (February and March). It increases again in April to above 40 km before its transition to a complex vertical structure in summer months. For example, in May, it has a 6 h phase change near 90 km, below which it has downward phase progression but becomes independent of height above; in June, it has upward progression from 85 to 92 km but, again, becomes height-independent above 92 km. All these irregularities in the tidal phase profiles are possibly due to interference between propagating and evanescent components of the diurnal temperature oscillation during
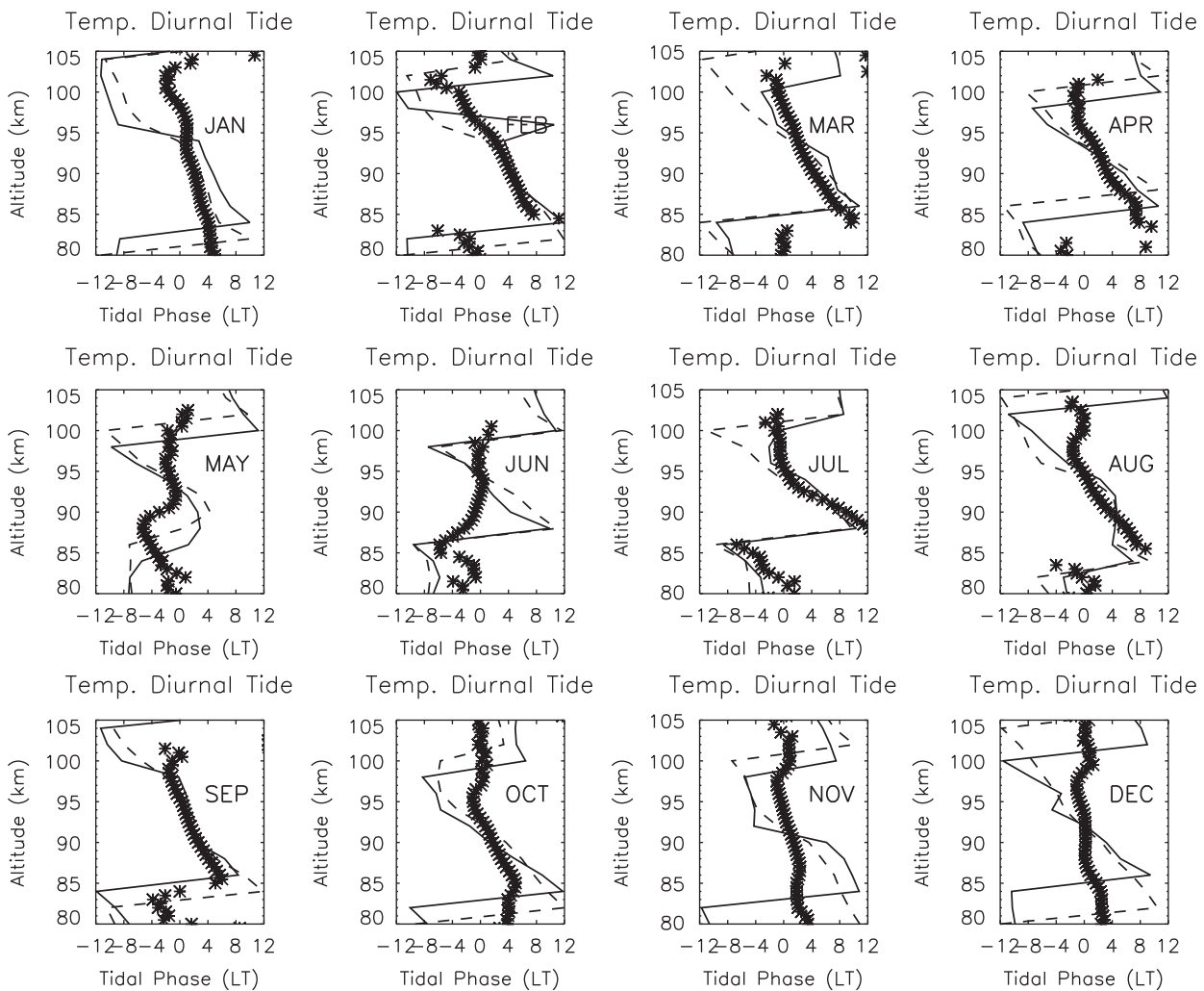
Fig. 2. Diurnal phase profiles associated with Fig. 1.

summer. The diurnal phase profile changes back to propagating behavior (tilted phase profile with downward phase progression) during July and August with shorter vertical wavelengths (near 25 km). Approaching fall equinox (September), the lidar-observed diurnal tidal vertical wavelength starts to increase again (to near 40 km), but it still shows propagating behavior. The evanescent tidal character appears at both the upper and lower limits of the mesopause region in October, but maintains propagating character between 85 and 95 km with slightly longer vertical wavelength (around 50 km) than that of September. However, it exhibits evanescent character with very long vertical wavelength in November and December having constant phase near 0100 local time. Since the Na lidar observations enjoyed high signal-to-noise ratios from late fall through winter, the associated photon noise errors are minimal during this time of the year. Due mainly to day-to-day variability, the resulting uncertainty of the best fit lidar temperature monthly mean diurnal amplitude is less than 1 K between 80 and 100 km in winter and between 84 and 95 km in summer months. Since the photon noise of lidar measurements is also altitude dependent, the amplitude uncertainly is about 0.7 K at the sodium peak and increases quickly beyond the indicated altitude ranges.

Compared to the lidar results, SABER observed somewhat shorter vertical wavelengths in January within the altitude range of 84 to 94 km, along with a 12-h phase shift near 95 km. The phase profile of SABER in February is quite similar to that of

January, and also agrees well with lidar profile below 94 km in the same month. Although the SABER diurnal tide corresponds to a propagating mode in March and April, its vertical wavelength (20~25 km) is, again, shorter than what the lidar measured (30~40 km). There is a difference in May and June between the phases observed by the two instruments: lidar showing dominance of evanescent behaviors, while above ~90 km SABER observing propagating behavior. On the other hand, from July to September, the SABER tidal phase and amplitude profiles overlap with lidar profiles extremely well with similar vertical phase gradient. For the rest of the year (October to December), unlike the lidar which observed very long vertical wavelength, SABER observed diurnal tidal phase profiles still showing a propagating character except in November. The November phase profile of SABER is quite complex. Between 92 and 98 km, the vertical wavelength is also quite long and about the same as the lidar observation. Below 90 km, the SABER observed vertical wavelength is around 50 km, which is still about twice as long as than those observed in equinoctial months.

In summary, the lidar observed diurnal tidal temperature consists of a combination of evanescent (trapped) and propagating characteristics. During summer, the tidal phases show trapped behavior above 90 km, and it is mainly propagating during equinoctial months with the vertical wavelength varying from 20 to 40 km. The lidar observed evanescent diurnal phase in winter months appears contrary to model predictions and the

SABER observations, which show the propagating tidal wave behavior all year long with relatively small seasonal variations.

3.2. Migrating diurnal tide observed by SABER at $40°N$ and $255°E$

To further understand the tidal wave activity over Fort Collins, CO, it would be very helpful if the relative contributions of migrating and nonmigrating tides can be identified. With the unprecedented temperature measurements from the SABER instrument from space, one is able to separate and diagnose the global contributions between the migrating and nonmigrating temperature tidal waves, thereby helping to assess their relative contributions in observed tidal-period perturbations at a local (lidar) site. In Fig. 1, we also showed the diurnal tidal amplitudes for westward wavenumber 1 component (DW1), which is the migrating or Sun-synchronous component of the diurnal tide, deduced from SABER data for each month. Although not shown, the SABER tidal results reveal that the migrating amplitude is much larger than the nonmigrating diurnal tidal components (most of their amplitudes are close or less than 1 K within the mesopause region during most part of the year at this location). So, it is not surprising to see that the DW1 amplitude (dash lines in Fig. 1) and phase profiles (dash lines in Fig. 2) show very small difference from the total reconstructed diurnal tide (solid lines) within the lidar detection range (80–105 km). However, the considerable difference between the SABER total diurnal tide profiles and lidar observations during winter and early spring may imply that DW1 (migrating tide) may not be the dominant contributor to the temperature diurnal tidal period perturbation observed by the CSU Na lidar in this part of the year. Since SABER cannot observe short-term tidal variability, the nonmigrating tidal variability due to the change in convective activity and nonlinear interaction included in the lidar observations, cannot be captured by the 60-day averaged SABER observation. This observational difference in day-to-day nonmigrating tidal variability may be the main reason for the observed difference of temperature diurnal tidal component in winter and early spring between the two instruments. It is interesting to note that earlier satellite observations of temperature diurnal tide by Microwave Limb Sounder (MLS) experiment on UARS satellite (Forbes and Wu, 2006) did indicate that the trapped DS0 (Diurnal Stationary wavenumber zero) and DW2 (Diurnal Westward wavenumber two) components seem to be stronger than the other nonmigrating diurnal tides and have high year-to-year variations near midlatitudes. The DE3 component, on the other hand, although quite strong within the equatorial region, does not appear to have significant amplitude near middle and high latitudes.

3.3. Na lidar observed anomalous tidal period oscillation in winter

To test the consistency of the lidar-observed evanescent temperature diurnal tide in winter months, we plot the amplitude and phase profiles in winter months, November, December and January, of each year, from 2002 to 2008 in Fig. 3. As the figure shows, although the winter diurnal tidal amplitude shows big year to year variations (for example, in January at 98 km, it varies from 10 K in 2003 to near 1 K in 2008 and 2007), its diurnal phase during the same winter month in different years behaves quite similarly (no clean downward phase progression). It is worth mentioning here that a similar vertical tidal phase profile,
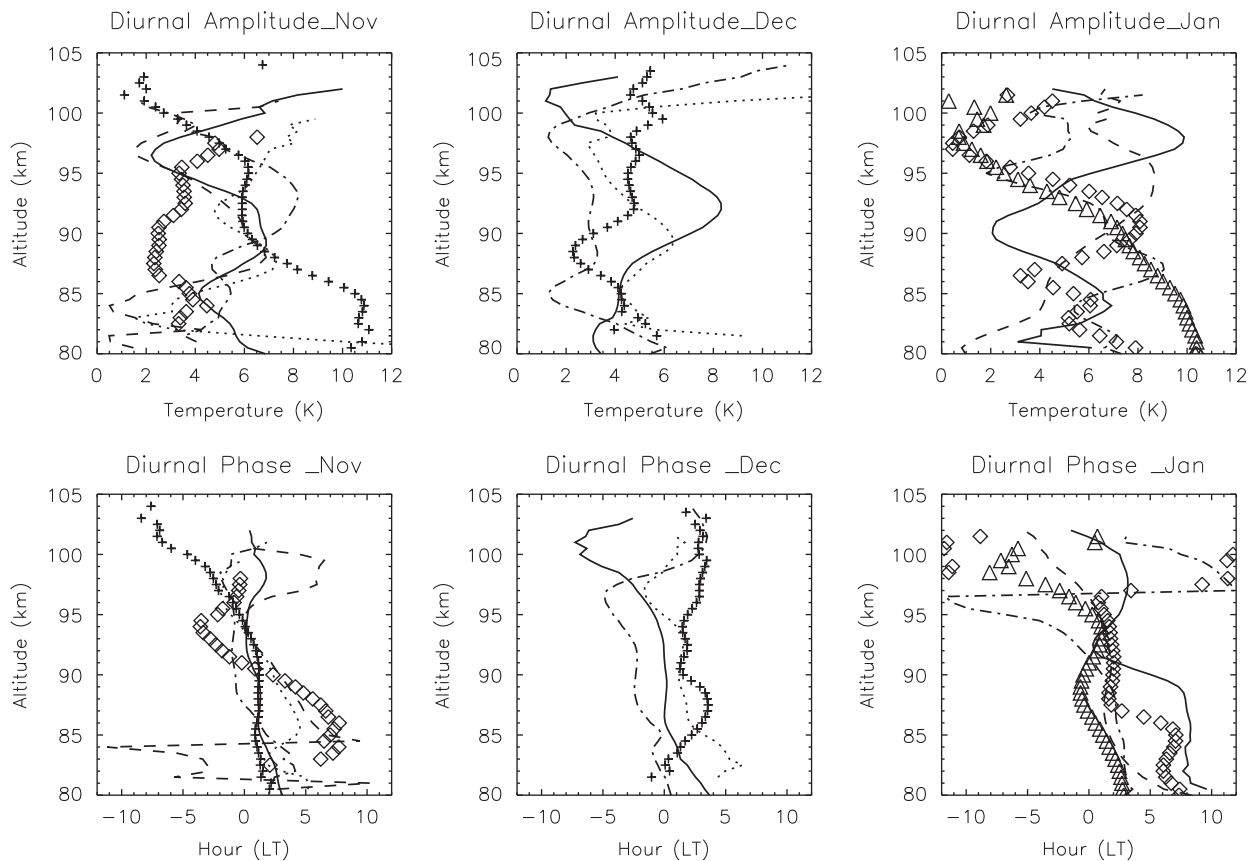
Fig. 3. CSU Na lidar-observed monthly averaged temperature diurnal amplitudes (top row) and phases (bottom row) of November (left column), December (middle column) and January (right column) for each year, from 2002 (plus sign), 2003 (solid line), 2004 (dotted line), 2005 (dashed line), 2006 (dash dot line), 2007 (triangles) and 2008 (diamonds).

exhibiting evanescent behavior, was also observed in December of 1998 by the CSU Na lidar (She et al., 2002). In November, some of the diurnal phase profiles do show propagating characteristics, especially the one in the November of 2008, when it shows typical propagating wave characteristic with vertical wavelength of 20 km, but a much smaller amplitude of 2–3 K compared to the rest of lidar measurements in Fig. 3. Looking back to Figs. 1 and 2, the amplitude and phase profiles of November 2008 are similar to those of the SABER total tidal profiles in November. In December and January, the diurnal phase profiles all show evanescent behavior with a nearly constant phase near midnight. We also note phase jumps or disturbances in the phase profiles in some January observations accompanied by wavy amplitude profiles. This lidar observed behavior may be the indication of some interference pattern. This interference could be either caused by two or more diurnal Hough modes or by migrating and nonmigrating tidal components. However, it is extremely difficult to uncover the real mechanism from the measurements at a single location. At the same time, although the year-to-year variations of the reconstructed diurnal amplitudes from SABER measurements in winter months (not shown) are similar in magnitude to the lidar amplitude profiles (top row of Fig. 3), the reconstructed phase profiles are highly variable. For example, the reconstructed diurnal phase profile for December of 2003 from SABER is extremely similar to the lidar observation within the mesopause region, but the phase profile for December 2006 of SABER are out of phase relative the lidar profile.

To further evaluate this anomalous behavior, we show in Fig. 4 the Lomb periodogram analysis on 4 data sets of Na lidar diurnal cycle observations in December to estimate the significance levels of the tidal period oscillation signals. The resulting Lomb power (Press et al., 1992) at the tidal periods, qualitatively mirrors the corresponding tidal amplitudes deduced from the harmonic analysis. A salient feature of the Lomb power lies in the fact that a Monte Carlo simulation with the same temporal structure may be used to assign a percent probability that a given Lomb power could be produced by random noise, thus giving an estimate of the significance level of the deduced Lomb power. In this connection, we use the % confidence defined as one minus the significance probability resulting from random noise, to represent the goodness of the tidal component. For each data set, we typically evaluate the Lomb powers required to give 50% (solid line), 95% (dash line) and 99.5% (dot dash line) confidence in the analysis. For example, in Fig. 4, we provide the Lomb power contours for four multi-day Na lidar continuous measurements in December. The calculated diurnal phase for each campaign is also plotted in the figure. It is clear that at altitudes where the diurnal signal is strong, a constant phase profile (around 24 h or midnight local time) emerges. The contour plots in (a), (b) and (c) are lidar measurements in December 2003, but separated by time gaps of close to one day between the first two campaigns and of about three days between the second and third campaign. The plot (d) in Fig. 4 represents another December lidar measurement in 2004, which was a continuous three-day observation from December 3–6. This contour exhibits extremely similar structure as plot (b) with significant 24-h period signal near 90 km (above 99.5% confidence level, in other words, there is less than 0.5% of chance that this signal is generated from random noise), except that the oscillation period is close to 26 h. However, from plot (a) through plot (c), it is evident that, within the same month of the same
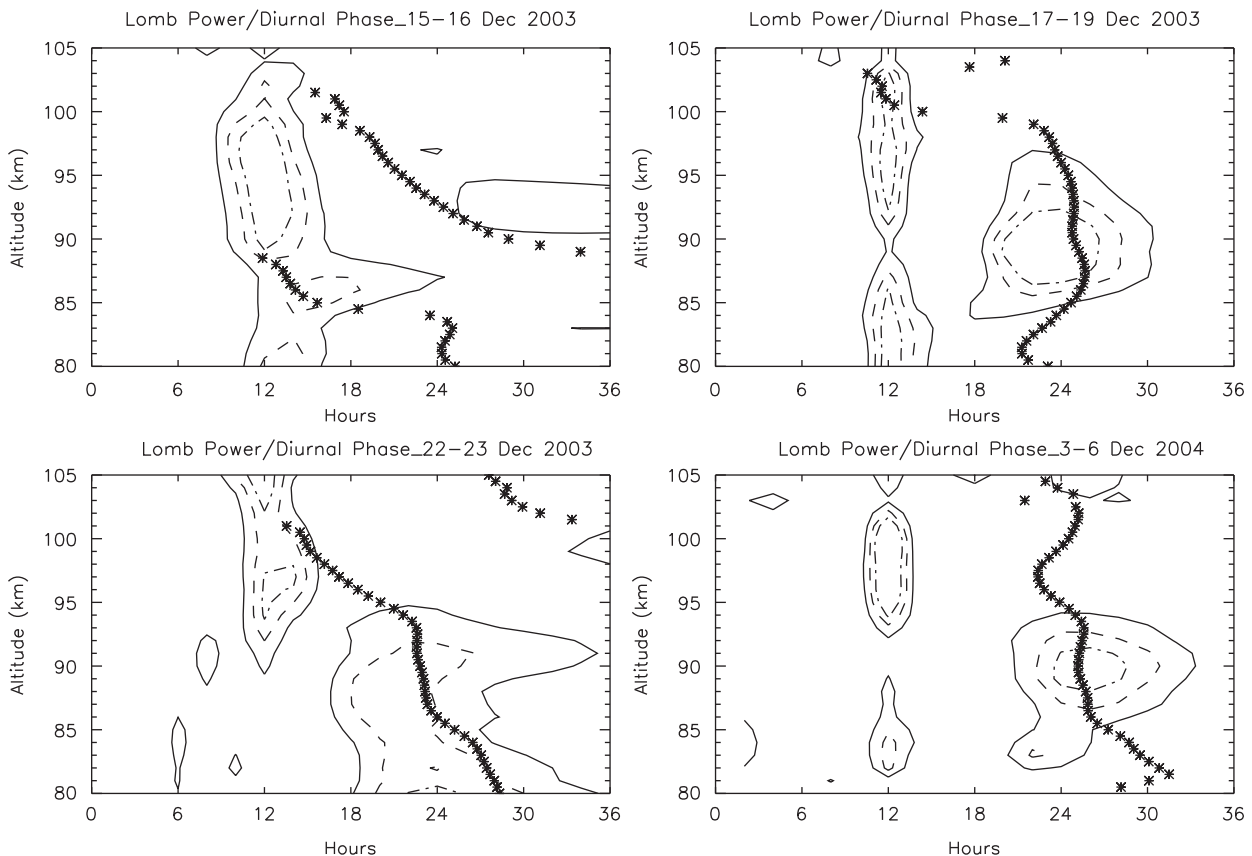
Fig. 4. Lomb power contour plots of four CSU Na lidar full-diurnal-cycle temperature observations (a: from December 15th to 16th of 2003; b: from December 17th to 19th of 2003; c: from December 21st to 22nd of 2003; d: from December 3rd to 6th of 2004), along with the diurnal phase profiles for each observations. The contour lines correspond to the power of Lomb periodogram that give 50% (solid line), 95% (dash line) and 99.5% (dash dot line) confidence for the deduced diurnal amplitude, plotted against period in hour. The asterisks show the corresponding diurnal tidal phases in hour (LT).

year, such 24-h oscillations are quite variable. It was quite weak (below 50% confidence level with peak amplitude near 5 K) in the first 30-h campaign (December 15–16). However, about 18 h later, this diurnal period signal became significant (above 99.5% confidence level and peak amplitude of 9 K near 90 km) during the second lidar campaign (December 17–19). In a campaign (December 22–23) that started a few days later, this oscillation signal, although it was still above 95% confidence level, was weakened with amplitude near 8 K around 90 km and the period was only approximately 24-h. Similar variability is also evident in November and January. Thus, this diurnal period signal in the lidar observation, though robust enough to consistently exhibit evanescent diurnal tidal phase in the monthly mean, has considerable day-to-day variations and irregularity within the winter months. This could be the principal reason that the SABER instrument misses this winter feature, since it can only capture consistent tidal wave activities over periods of about 60 days. We note that compared with this 24-h period signal, the 12-h period oscillation is much more significant and consistent for every lidar observation (also shown in Fig. 4) and every year, mostly because the semidiurnal tidal amplitude reaches its maximum in winter at midlatitudes (Forbes et al., 2008). This may be the reason why the semidiurnal amplitude and phase comparisons (not shown) between the observations of the CSU Na lidar and SABER yields greater agreement all year long. It is puzzling to note that the simultaneous zonal wind diurnal tide lidar observations do not reveal such robust quasi-trapped tidal wave behavior (meridional wind diurnal tidal amplitudes in the winter months are too small to generate meaningful phase values), but a propagating behavior that is in good agreement with model predictions and radar measurements in midlatitudes (Yuan et al., 2006).

4. Discussion

The features of propagating diurnal tidal behavior observed by lidar near equinox, and trapped modes dominance during solstice are in qualitative agreement with an earlier numerical experiment by Forbes and Hagan (1988) accounting for atmospheric mean wind and dissipation effects on migrating diurnal tide propagation. They found that the difference in diurnal tidal behavior between solstice and equinox seasons are most likely due to the seasonal variations of atmospheric dissipation (Garcia and Solomon, 1985 and Khattatov et al., 1997) with maximum dissipation and significant mean wind asymmetry about the equator under solstice conditions. Unlike classical linear tidal theory, this simulation with dissipation reveals a spreading of tidal oscillations to middle and higher latitudes instead of being confined near the equatorial region. Such broadening to higher latitude of the diurnal tide could be interpreted as the dominate Hough mode (1, 1) coupling into the first symmetric and asymmetric evanescent Hough modes $(1, -2)$ and $(1, -1)$ and, therefore, increasing the total tidal vertical wavelength. At the same time, the large dissipation factor during the solstice condition could excite more evanescent modes via the mode coupling mechanism and, therefore, could make evanescent mode prevail around solstices. Unfortunately, due to limitation of TIMED satellite's yaw cycle period, SABER cannot provide enough tidal analysis poleward beyond $50°$, where the major diurnal trapped modes prevail, making it extremely difficult to estimate their characteristics. In any event, Forbes and Wu (2006) did find that trapped modes made important contributions to DW1 at middle and high latitudes at 86 km by using the MLS experiment on board the UARS satellite. Although mode coupling-induced tidal structure broadening (Lindzen and Hong, 1974; Lindzen et al., 1977; Forbes and Hagan, 1988) could explain some

observed diurnal trapped mode behavior in the mesopause region above Fort Collins during solstice conditions, we cannot exclude the possibility of tidal forcing contributions from in situ mesospheric ozone heating (Marsh et al., 2002) or chemical heating (Mlynczak and Solomon, 1993, Smith et al., 2003).

On the other hand, the nonlinear interaction between the migrating diurnal tide and stationary planetary wave with wavenumber one (SPW1) can produce trapped diurnal tidal components of DS0 and DW2 (Hagan and Roble, 2001). SPW1 peaks in the northern hemisphere winter and early spring at middle and high latitudes, and it is intriguing to notice that it is also the same time of the year when the lidar observes considerably larger diurnal amplitude than SABER observations and anomalous diurnal phase behavior. However, due to the relative short life time of this planetary wave (compared with 60 days of sampling needed by SABER), it is difficult for the SABER instrument to capture such tidal variability.

It is also possible that the "anomalous" diurnal tidal behavior in winter is produced by some tidal-gravity wave interactions (Walterscheid, 1981). Based on Walterscheid's numerical simulations, such interaction would greatly enhance the tidal amplitude, and cause a change in tidal phase behavior below and near the critical level. Below the critical level, it would shorten the vertical wavelength of the tide. Near the critical level, the interaction would lengthen the tidal wave's vertical wavelength, leading to the appearance of a constant phase profile, sometimes termed the "pseudo tide". The tidal-gravity wave interaction is expected to occur locally with significant day-to-day variation and irregular occurrence. However, the lidar observed monthly mean tidal phase with evanescent behavior is quite robust, as it appears in almost every year's winter months, including temperature observations in the late 1990s (She et al., 2002). The complete story for the lidar observed winter anomaly and the difference between lidar and SABER observations in winter months await a more focused investigation in the future.

5. Conclusions

Since Na lidar in Colorado State University achieved the capability of simultaneously measuring neutral temperature, zonal wind, and meridional wind within the mesopause region over a full diurnal cycle in May 2002, we collected nearly 5000 h of such data by the end of 2008. The diurnal and semidiurnal tidal period perturbations of each of these atmospheric dynamic parameters within this layer of atmosphere above Fort Collins, CO ($41°N$, $105°W$) are then deduced. The launching of TIMED/ SABER instrument and its 3-D global temperature mapping has achieved an unprecedented view of solar thermal tidal activities around the globe from 20 to 120 km in altitude, providing local ground stations new opportunities to evaluate and understand their local tidal observations. In this paper, the mesopause region seasonal variations of temperature diurnal tide observed by the two instruments above Fort Collins are compared and studied. For most part of the year (April to October), the tidal amplitude measurements by SABER and Na lidar show good agreement. However, lidar observed considerably larger diurnal amplitudes in winter and early spring than those of SABER. Although both diurnal amplitude observations show summer minimum of 2–3 K, the lidar observed diurnal amplitude shows a strong annual variation and has a significant maximum in February near 90 km altitude with the peak value of 12 K, whereas the SABER diurnal amplitude shows semiannual variation with two maxima near spring and fall equinox of a value around 7 K. The diurnal phase profiles of the two instruments are again extremely similar during most part of the year with a downward phase progression, except

in the winter months, as well as in June, when the lidar observed "evanescent wave" behavior with the diurnal phase profiles showing very long or infinite vertical wavelength. This near evanescent characteristic with constant phase near midnight was observed in almost every winter from 2002 to 2008, when the lidar was operating, except in November 2008. The SABER-detected tidal phase, however, shows propagating behavior with downward progression all year long.

Although an early numerical experiment study by Forbes and Hagan (1988) suggested that atmospheric dissipation prompts the coupling of dominate (1, 1) mode into evanescent modes and broadening the latitudinal structure of diurnal tide, we cannot rule out the possibility of the nonlinear interaction between the migrating diurnal tide and planetary wave, such as stationary planetary wave, and tidal-gravity wave interactions. Both tend to lengthen the vertical wavelength of diurnal tide and are more active in winter months. All these tide-wave nonlinear interactions generate some highly variable nonmigrating tidal components with long vertical wavelength and, therefore, cause large tidal variability of the total tide observed by a ground-based instrument. The weakening of migrating diurnal tide in solstice condition could make those nonmigrating tides more pronounced in local tidal observations. However, the exact cause of the temperature diurnal phase anomaly observed by lidar cannot be presently determined. Since the observed phenomena is very robust, occurring every winter the lidar had data, more observations and further investigations are necessary to fully understand this anomaly.

Acknowledgement

Reference

Avery, S.K., Vincent, R.A., Phillips, A., Manson, A.H., Fraser, G.J., 1989. High latitude tidal behavior in the mesosphere and lower thermosphere. J. Atmos. Terr. Phys. 51, 595–608.

Chapman, S., Lindzen, R.S., 1970. Atmospheric Tides. Gordon and Breach, New York, pp. 200.

Forbes, J.M., Garrett, H.B., 1978. Thermal excitation of atmospheric tides due to insolation absorption by O_3 and H_2O. Geophys. Res. Lett. 5 (12), 1013–1016.

Forbes, J.M., Garrett, H.B., 1979. Theoretical studies of atmospheric tides. Rev. Geophys. Space Phys. 17, 1951–1981.

Forbes, J.M., 1982a. Atmospheric tides, 1, model description and results for the solar diurnal component. J. Geophys. Res. 87 (A7), 5222–5240.

Forbes, J.M., 1984. Middle atmosphere tides. J. Atmos. Terr. Phys. 46, 1049–1067.

Forbes, J.M., Hagan, M.E., 1988. Diurnal propagating tide in the presence of mean winds and dissipation: a numerical investigation. Planet. Space. Sci. 36 (6), 579–590.

Forbes, J.M., 1995. Tidal and planetary waves, in The Upper Mesosphere and Lower Thermosphere. In: Johnson, R.M., Killeen, T.L. (Eds.), A Review of Experiment and Theory, Geophys. Monogr. Ser., vol. 87. AGU, Washington, DC, pp. 67–87.

Forbes, J.M., Hagan, M.E., Zhang, X., Hamilton, K., 1997. Upper atmospheric tidal oscillations due to latent heat release in the tropical troposphere. Ann. Geophys. 15, 1165–1175.

Forbes, J.M., Wu, D., 2006. Solar tides as revealed by measurements of mesosphere temperature by the MLS experiment on UARS. J. Atmos. Sci. 63 (7), 1776–1797.

Forbes, J.M., Zhang, X., Palo, S., Russell, J., Mertens, C.J., Mlynczak, M., 2008. Tidal variability in the ionospheric dynamo region. J. Geophys. Res. 113, A02310, doi:10.1029/2007JA012737.

Franke, S.J., Thorsen, D., 1993. Mean winds and tides in the upper middle atmosphere at Urbana (40oN, 88oW) during 1991–92. J. Geophys. Res. 98, 18607–18615.

GarcíaComas, M., Lopez-Puertas, M., Marshall, B.T., Wintersteiner, P.P., Funke, B., Bermejo-Pantaleon, D., Mertens, C.J., Remsberg, E.E., Gordley, L.L., Mlynczak, M.G., Russel, J.M., 2008. Errors in Sounding of the Atmosphere using Broadband Emission Radiometry (SABER) kinetic temperature caused by non-local-thermodynamic-equilibrium model parameters. J. Geophys. Res. 113, D24106, doi:10.1029/2008JD010105.

Garcia, R.R., Solomon, S., 1985. The effect of breaking gravity waves on the dynamics and chemical composition of the mesosphere and lower thermosphere. J. Geophys. Res. 90, 3850–3868.

Hagan, M.E., 1996. Comparative effects of migrating solar sources on tidal signatures in the middle and upper atmosphere. J. Geophys. Res. 101 (D16), 21,213–21,222, doi:10.1029/96JD01374.

Hagan, M.E., Chang, J.L., Avery, S.K., 1997. GSWM estimates of nonmigrating tidal effects. J. Geophys. Res. 102, 16439–16452.

Hagan, M.E., Burrage, M.D., Forbes, J.M., Hackney, J., Randel, W.J., Zhang, X., 1999. GSWM-98: results for migrating solar tides. J. Geophys. Res. 104 (A4), 6813–6827, doi:10.1029/1998JA900125.

Hagan, M.E., 2000. In: Siskind, D.E., Echermann, S.D., Summers, M.E. (Eds.), Atmospheric Tidal Propagation Across the Stratopause, Atmospheric Science Across the Stratopause, Geophys. Monogr. Ser., vol. 123. AGU, Washington, DC, pp. 177–190.

Hagan, M.E., Roble, R.G., 2001. Modeling diurnal tide variability with the National Center for Atmospheric Research the mesosphere–ionosphere–mesosphere-electrodynamics general circulation model. J. Geophys. Res. 106 (24), 869–24882.

Hagan, M.E., Forbes, J.M., 2002. Migrating and nonmigrating diurnal tides in the middle and upper atmosphere excited by tropospheric latent heat release. J. Geophys. Res. 107 (D24), 4754, doi:10.1029/2001JD001236.

Hong, S.-S., Wang, P.-H., 1980. On the thermal excitation of atmospheric tides. Bull. Geophys. Natl. Cent. Taiwan 19, 56–83.

Kato, S., 1980. Dynamics of the Upper Atmosphere. Center for Academic Publications, Tokyo.

Khattatov, B.V., Geller, M.A., Yubin, V.A., Hays, P.B., 1997. Diurnal migrating tide as seen by the high-resolution Doppler imager/UARS, 2. Monthly mean global zonal and vertical velocities, pressure, temperature, and inferred dissipation. J. Geophys. Res. 102 (D4), 4423–4435.

Lieberman, R.S., Oberheide, J., Hagan, M.E., Remsberg, E.E., Gordley, L.L., 2004. Variability of diurnal tides and planetary waves during November 1978–May 1979. J. Atmos. Sol.-Terr. Phys. 66, 517–528.

Lindzen, R.S., Hong, S.-S., 1974. Effects of mean winds and horizontal temperature gradients on solar and lunar semidiurnal tides in the atmosphere. J. Atmos. Sci. 31, 1421–1446.

Lindzen, R.S., Hong, S.-S., Forbes, J.M., 1977. Semidiurnal Hough Mode Extensions into the Thermosphere and their Applications. Memo. Rep. 3442, Naval Research Laboratory, Washington, DC 65 pp.

Lindzen, R.S., 1978. Effect of daily variations of cumulonimbus activity on the atmospheric semidiurnal tide. Mon. Weather Rev. 106, 526–533.

Liu, H.-L., Li T., She C.-Y., Oberheide J., Wu Q., Hagan M. E.,Xu J., Roble R. G., Mlynczak M. G., and J. M. Russell III (2007), Comparative study of short term diurnal tidal variability, J. Geophys. Res., 10.1029/2007JD008542.

Manson, A.H., Meek, C.E., Teitelbaum, H., Vial, F., Schminder, R., Kuschner, D., Smith, M.J., Fraser, G.J., Clark, R.R., 1989. Climatologies of semi-diurnal and diurnal tides in the middle atmosphere (70–110 km) at middle latitudes (40–50). J. Atmos. Terr. Phys. 51, 579–593.

Marsh, D.R., Skinner, W.R., Marshall, A.R., Hays, P.B., Ortland, D.A., Yee, J.-H., 2002. High resolution Doppler Imager observations of ozone in the mesosphere and lower thermosphere. J. Geophys. Res. 107 (D19), 4390, doi:10.1029/2001JD001505.

Mayr, H.G., Mengel, J.G., Talaat, E.R., Porter, H.S., Chan., K.L., 2003. Non-migrating diurnal tides generated with planetary waves in the Mesosphere. Geophys. Res. Lett. 30 (16, doi:10.1029/2003GL017877.

Mayr, H.G., Mengel, J.G., Chan, K.L., Porter, H.S., 2001. Mesosphere dynamics with gravity wave forcing: Part I. Diurnal and semi-diurnal tides. J. Atmos. Sol.-Terr. Phys 63, 1851–1864.

McLandress, C., 2002. The seasonal variation of the propagating diurnal tide in the mesosphere and lower thermosphere. Part II: the role of tidal heating and zonal mean winds. J. Atmos. Sci. **59**, 907–922.

Mclandress, C., 2001. The seasonal variation of the propagating diurnal tide in the mesosphere and lower thermosphere, Part I, the role of gravity waves and planetary waves. J. Atmos. Sci. 59, 893–906.

Mclandress, C., Ward, W.E., 1994. Tidal/gravity wave interactions and their influence on the large-scale dynamics of the middle atmosphere: model results. J. Geophys. Res. 99, 8139–8155.

Mertens, C.J., Mlynczak, M.G., LópezPuertas, M., Wintersteiner, P.P., Picard, R.H., Winick, J.R., Gordley, L.L., Russell, J.M., 2001. Retrieval of mesospheric and lower thermospheric kinetic temperature from measurements of CO_2 15 μm earth limb emission under non-LET conditions. Geophys. Res. Lett. 28, 1391–1394.

Mertens, C. J. F. J. Schmidlin, R. A. Goldberg, E. E. Remsberg, W. D. Pesnell, J. M. Russel, M. G. Mlynczak, M. L. Puertas, P. P. Wintersteiner, R. H. Winick, L. L.Gordley (2004), SABER observations of mesospheric temperature and comparisons with falling sphere measurements taken during the 2002 summer MaCWINE campaign, Geophys. Res. Lett., 31, J03105, 10.1029/2003GL018605.

Miyahara, S., Miyoshi, Y., 1997. Migrating and nonmigrating atmospheric tides simulated by a middle atmosphere general circulation model. Adv. Space Res. 20, 1201–1207.

Mlynczak, M.G., Solomon, S., 1993. A detailed evaluation of heating efficiency in the middle atmosphere. J. Geophys. Res. 98 (D6), 10517–10541, doi:10.1029/93JD00315.

Oberheide, J., Wu, Q., Killeen, T.L., Hagan, M.E., Roble, R.G., 2006. Diurnal nonmigrating tides from TIMED Doppler Interferometer wind data: monthly

climatologies and seasonal variations. J. Geophys. Res. 111, A10S03, doi:10.1029/2005JA011491.

Press, W.H., Teukolsky, S.A., Vetterling, W.T., Flannery, B.P., 1992. In: Press, W.H. (Ed.), Numerical Recipes, in C: The Art of Scientific Computing 2nd ed. Cambridge Univ. Press, New York, pp. 575 sect. 13.8.

Remsberg, E.E.B.T., Marshall, M., Garcia-Comas, D., Krueger, G.S., Lingerfelser, J., Martin-Torres, M.G., Mlynczak, J.M., Russell, A.K., Smith, Y., Zhao, C., Brown, L.L., Gordley, M.J., Lopez-Gonzalez, M., Lopez-Puretas, C-Y., She, M.J., Taylor, R.E., Thompson, 2008. Assessment of the quality of the Version 1.07 temperature-versus-pressure profiles of the middle atmosphere from TIMED/SABER. J. Geophys. Res. 113, D17101, doi:10.1029/2008JD010013.

She, C.Y., Chen, S., Williams, B.P., Hu, Z., Krueger, D.A., Hagan, M.E., 2002. Tides in the mesopause region over Fort Collins, CO (41°N, 105°W) based on lidar temperature observations covering full diurnal cycles. J. Geophys. Res. 107 (D18), 4350, doi:10.1029/2001JD001189.

She, C.Y., Sherman, J., Yuan, T., Williams, B.P., Arnold, K., Kawahara, T.D., Li, T., Xu, L.F., Vance, J.D., Acott, P., Krueger, D.A., 2003. The first 80-h continuous lidar campaign for simultaneous observation of mesopause region temperature and wind. Geophys. Res. Lett. 30 (6), 52, doi:10.1029/2002GL016412.

Smith, A.K., Marsh, D.R., Szymczak, A.C., 2003. Interaction of chemical heating and the diurnal tide in the mesosphere. J. Geophys. Res. 108 (D5), 4164, doi:10.1029/2002JD002664.

Talaat, E.R., Lieberman, R.S., 1999. Nonmigrating diurnal tides in mesospheric and lower-thermospheric winds and temperatures. J. Atmos. Sci. 56, 4073–4087.

Tsuda, T., Kato, S., Manson, A.H., Meek, C., 1988. Characteristics of semidiurnal tides observed by the Kyoto meteor radar and Saskatoon medium-frequency radar. J. Geophys. Res. 93, 7027–7036.

Vincent, R.A., Tsuda, T., Kato, S., 1989. Asymmetries in mesospheric tidal structure. J. Atmos. Terr. Phys. 51, 609–616.

Volland, H., 1988. Atmospheric Tidal and Planetary Waves. Kluwer Academic Publishers, Norwell, Mass.

Walterscheid, R.L., 1981. Inertio-gravity wave induced accelerations of mean flow having an imposed periodic component: implications for tidal observations in the Meteor Region. J. Geophys. Res. 86 (C10), 9698–9706.

Wu, Q., Ortland, D.A., Killeen, T.L., Roble, R.G., Hagan, M.E., Liu, H.-L., Solomon, S.C., Xu, Jiyao, Skinner, W.R., Niciejewski, R.J., 2008. Global distribution and interannual variations of mesospheric and lower thermospheric neutral wind diurnal tide: 2. Nonmigrating tide. J. Geophys. Res. 113, A05309, doi:10.1029/2007JA012543.

Xu, J., She, C.Y., Yuan, W., Mertens, C., Mlynczak, M., Russell, J., 2006. Comparison between the temperature measurements by TIMED/SABER and lidar in the midlatitude. J. Geophys. Res. 111, A10S09, doi:10.1029/2005JA011439.

Yuan, T., She, C.Y., Hagan, Maura E., Williams, B.P., Li, Tao, Arnold, Kam, Kawahara, Takuya D., Acott, P.E., Vance, J.D., Krueger, D.A., Roble, R.G., 2006. Seasonal variation of diurnal perturbations in mesopause region temperature, zonal, and meridional winds above Fort Collins, Colorado (40.6°N, 105°W). J. Geophys. Res. 111, D06103, doi:10.1029/2004JD005486.

Yuan, T., She, C.-Y., Krueger, D.A., Sassi, F., Garcia, R., Roble, R.G., Liu, H.-L., Schmidt, H., 2008a. Climatology of mesopause region temperature, zonal wind, and meridional wind over Fort Collins, Colorado (41°N, 105°W), and comparison with model simulations. J. Geophys. Res. 113, D03105, doi:10.1029/2007JD008697.

Yuan, T., Schmidt, H., She, C.Y., Krueger, D.A., Reising, S., 2008b. Seasonal variations of semidiurnal tidal perturbations in mesopause region temperature and zonal and meridional winds above Fort Collins, Colorado (40.6°N, 105.1°W). J. Geophys. Res. 113, D20103, doi:10.1029/2007JD009687.

Zhang, X., Forbes, J.M., Hagan, M.E., Russell III, J.M., Palo, S.E., Mertens, C.J., Mlynczak, M.G., 2006. Monthly tidal temperatures 20–120 km from TIMED/SABER. J. Geophys. Res. 111, A10S08, doi:10.1029/2005JA011504.